Acta Mechanica 136, 17–27 (1999)

ACTA MECHANICA

Numerical studies of three turbulent slot jets with and without moving surface

Y.-T. Yang and **T.-P. Hao,** Tainan, Taiwan

(Received May 11, 1998; revised June 9, 1998)

Summary. This study presents the numerical predictions of the fluid flow and heat transfer characteristics for three turbulent impingement slot jets. The turbulent governing equations are solved by a control-volume-based finite-difference method with power-law scheme, the well known K-ε model, and its associate wall function to describe the turbulent behavior. The velocity and pressure terms of momentum equations are solved by the SIMPLE (Semi-Implicit Method for Pressure-Linked Equation) method. In this study nonuniform staggered grids are used. The parameters interesting include entrance Reynolds number (Re), dimensionless nozzle to surface space (H/W), dimensionless pitch (P/W), and dimensionless velocity ratio (U_s/V_j). The computed results show that the dimensionless pitch has a strong influence on the heat transfer characteristics. In the case with surface motion, it is found that the skin friction coefficient of the impinging surface is strongly affected by the surface motion, but the heat transfer characteristic is not significant in the range of $0.05 \leq U_s/V_j \leq 0.25$.

Nomenclature

C_1, C_2, C_μ	turbulent constant
C_f	skin friction coefficient
E	constant
G	generation rate of turbulent kinetic energy
H	distance between the nozzle and the impingement surface
i	turbulence intensity
K	turbulent kinetic energy
Nu	local Nusselt number
P	pitch
q''	heat flux
Re	Reynolds number
S_ϕ	source term
T	temperature
U_τ	friction velocity
U_s	velocity of surface motion
V_j	jet velocity
U, V	x, y component velocity
W	nozzle width
y^+	dimensionless distance from the wall
ϕ	dependent variables
Γ_ϕ	diffusion coefficient of ϕ equation
α	thermal diffusivity of fluid
ϱ	density
κ	von Kármán constant
σ	turbulent Prandtl number

μ	dynamic viscosity
ν	kinematic viscosity
τ_w	wall shear stress
ε	turbulent energy dissipation rate
λ	length scale constant

1 Introduction

Impinging jets are often used to heat or cool a surface. The applications of the impingement technique include cooling of turbine blades, drying of paper, textiles, cooling of electrical equipment, and annealing of metals. Several numerical studies have been presented of a jet impinging on a flat plate. Wolfstein [1] solved the plane turbulent impinging jet by using a one-equation turbulence model. Bower et al. [2] applied a one-equation turbulence model to an axisymmetric jet impinging on a flat plate. Gosman et al. [3] and Spalding [4] used the one-equation model to recirculating flows, and the results agree well with the experiments. Agarwal and Bower [5] demonstrated the superiority of the two-equation model for lift-jet configurations over the simple models, namely the zero-equation and one-equation models. Detailed calculations of impinging jets have been attempted for single jet flows with or without cross flow by Huang et al. [6], Amano and Brandt [7], Chuang and Wei [8], and Chuang et al. [9]. In practice more than one nozzle is used when a larger part of the surface is to be heated or cooled. The two most frequently encountered jet configurations are circular jets and slot jets. The study to be reported in this paper is concerned with the latter. The basic difference of single and multiple jets precludes the use of single jet heat transfer results for the design of multiple jet heating or cooling systems. In 1992, Ichimiya [10] analyzed the characteristics of heat transfer and flow situation by confined three laminar slot jets. His calculations were constrained to a laminar jet. From a literature search it appears that there is very little information available on three turbulent slot jets. For three turbulent slot jets, the individual jets which comprise a multi-jet system may be influenced by two types of interactions which do not occur in the case of single jets. In this application, the lift jets interact strongly with the ground plane for a ground vortex that wraps around the impingement regions and an upwash fountain resulting from the collision of the wall jets. The flow pattern of three turbulent slot jets can be divided into six characteristics regions: i) free jet region ii) impinging region iii) wall jet region iv) fountain-formulation region v) fountain up-wash region vi) entrainment, as shown in Fig. 1. The present work is to extend the calculation to turbulent jets. The study of impinging three slot turbulent jets provides a basis for understanding the essential dynamics of multiple jets.

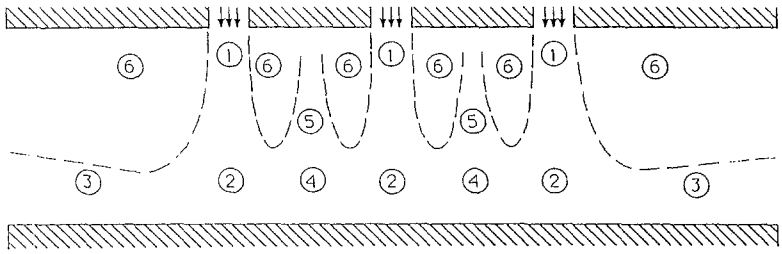

Fig. 1. The flow field characteristics of three turbulent slot jets

2 Mathematical formulation

In the present study, the flow is assumed to be steady, turbulent, and incompressible, and the properties of the fluid are assumed to be constant. The geometry and coordinate system are shown in Fig. 2. The steady conservation equations for incompressible two-dimensional Cartesian coordinates mean flow and thermal characteristics of turbulent flow can be written as

$$\frac{\partial}{\partial x}(\varrho U\phi)+\frac{\partial}{\partial y}(\varrho V\phi)=\frac{\partial}{\partial x}\left[\Gamma_\phi\frac{\partial\phi}{\partial y}\right]+\frac{\partial}{\partial y}\left[\Gamma_\phi\frac{\partial\phi}{\partial y}\right]+S_\phi\,, \tag{1}$$

where ϕ stands for the dependent variables U, V, K, ε, and T; U and V are local time-averaged velocity in x and y directions, respectively; Γ_ϕ and S_ϕ are the corresponding turbulent diffusion coefficient and source term Γ_ϕ respectively for general variable ϕ. The equations are summarized in Table 1. The turbulent viscosity μ_T and μ_e are expressed as follows:

$$\mu_T=\varrho C_\mu\frac{K^2}{\varepsilon}\,, \tag{2}$$

$$\mu_e=\mu_\ell+\mu_T=\mu_\ell+\varrho C_\mu\frac{K^2}{\varepsilon}\,. \tag{3}$$

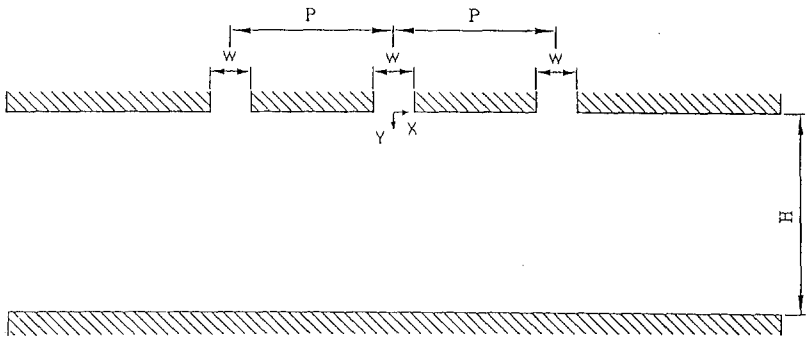

Fig. 2. Coordinate system

Table 1. Conservation equations

Equation	ϕ	Γ_ϕ	S_ϕ
Mass	1	0	0
X-momentum	U	μ_e	$-\frac{\partial P}{\partial X}+\frac{\partial}{\partial X}\left[\mu_e\frac{\partial U}{\partial X}\right]+\frac{\partial}{\partial Y}\left[\mu_e\frac{\partial V}{\partial X}\right]$
Y-momentum	V	μ_e	$-\frac{\partial P}{\partial Y}+\frac{\partial}{\partial X}\left[\mu_e\frac{\partial U}{\partial Y}\right]+\frac{\partial}{\partial Y}\left[\mu_e\frac{\partial V}{\partial Y}\right]$
Energy	T	$\frac{\mu_\ell}{\sigma_\ell}+\frac{\mu_T}{\sigma_T}$	0
Turbulent kinetic energy	K	$\mu_\ell+\frac{\mu_T}{\sigma_k}$	$G-\varrho\varepsilon$
Turbulent energy dissipation rate	ε	$\mu_\ell+\frac{\mu_T}{\sigma_\varepsilon}$	$\frac{\varepsilon}{K}(C_1G-C_2\varrho\varepsilon)$

where

$$G=\mu_T\left\{2\left[\left(\frac{\partial U}{\partial X}\right)^2+\left(\frac{\partial V}{\partial Y}\right)^2+\left(\frac{\partial U}{\partial Y}+\frac{\partial V}{\partial X}\right)^2\right]\right\}.$$

The present study uses the following set of turbulence constants:

$$C_\mu = 0.09, \quad C_1 = 1.44, \quad C_2 = 1.92,$$
$$\sigma_k = 1.00, \quad \sigma_\varepsilon = 1.30, \quad \sigma_T = 0.8. \tag{4}$$

Boundary conditions

The computational domain boundaries without and with surface motion are shown in Fig. 3a and Fig. 3b. The boundary conditions for the above set of governing equations are:

(i) inlet boundary (A–B), (C–D), (K–L)
At the inlet boundary, uniform flow conditions are imposed as follows:

$$U = U_{\text{in}}, \quad K = K_{\text{in}} = iU_{\text{in}}^2,$$
$$\varepsilon = \varepsilon_{\text{in}} = \frac{K_{\text{in}}^{3/2}}{\lambda W}, \quad T = T_{\text{in}}, \tag{5}$$

where i is the turbulence intensity, λ is the length scale constant, and W is the nozzle width.
(ii) wall boundary (B–C), (D–E), (F–G), (I–K) and (L–A)

In this study, the upper walls (B–C), (D–E), (I–K), and (L–A) are assumed adiabatic and the bottom wall (F–G) is assumed isothermal. The near-wall region was simulated by a two zone model, i.e., viscous sublayer and fully turbulent zone, and the wall function method was used to bridge the viscous sublayer. The wall function approach consists of the assumption that the grid points nearest to the solid wall, that is, at a distance y_p from the nearest wall, components parallel to the wall (U_p) obey the following equations:

$$\tau_w = \frac{\mu_\ell U_p}{y_p} \qquad \text{when} \quad y^+ < 11.63,$$
$$\tau_w = \kappa \varrho C_\mu^{1/4} K_p^{1/2} \frac{U_p}{\ln(Ey^+)} \qquad \text{when} \quad y^+ \geq 11.63, \tag{6}$$

where $y^+ = \dfrac{U_\tau y_p}{\nu}$.

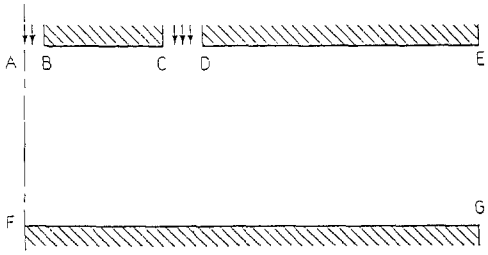

a

Fig. 3a. Boundary conditions without surface motion

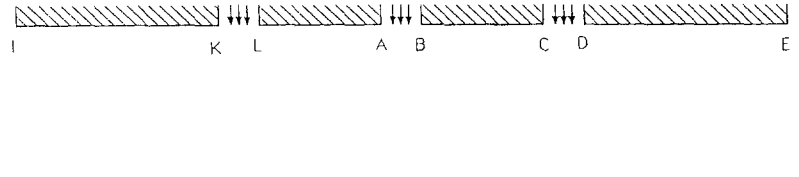

b

Fig. 3b. Boundary conditions with surface motion

K and ε were handled by the wall function proposed by Launder and Spalding [11],

$$\frac{(U_p - U_s)C_\mu^{0.25}K_p^{0.5}}{\tau_w/\varrho} = \frac{1}{\kappa}\ln\left[Ey_p\varrho\frac{(C_\mu^{0.5}K_p)^{0.5}}{\mu_\ell}\right], \tag{7}$$

$$K_p = \frac{U_\tau^2}{C_\mu^{1/2}} \quad \text{and} \quad \varepsilon_p = C_\mu^{3/4}\frac{K_p^{3/2}}{\kappa y_p}, \tag{8}$$

$$\frac{(T_p - T_s)\,C_p\varrho C_\mu^{0.25}K_p^{0.5}}{q_w''} = \sigma_T\left\{\left(\frac{1}{\kappa}\ln\left(Ey_p\varrho\frac{(C_\mu^{0.5}K_p)^{0.5}}{\mu_\ell}\right) + P\right)\right\}. \tag{9}$$

In addition, the temperature distribution T_p at point p is obtained from

$$\begin{aligned} T^+ &= \sigma \quad y^+ && \text{when} \quad y^+ < 11.63, \\ T^+ &= \sigma_T\left[\frac{1}{\kappa}\ln(Ey^+) + P\right] && \text{when} \quad y^+ \geq 11.63, \end{aligned} \tag{10}$$

where

$$T^+ = \frac{T_w - T}{T^*} \quad \text{and} \quad T^* = \frac{\alpha q_w''}{\kappa U_\tau}.$$

Jayetilleke [12] defined the experimental P function as

$$P = 9.24\left\{\left[\left(\frac{\sigma}{\sigma_T}\right)^{0.75} - 1\right] \times \left[1 + 0.28 \times \exp\left(-0.007 \times \frac{\sigma}{\sigma_T}\right)\right]\right\}. \tag{11}$$

The thermal boundary at wall (F–G):

$$T_{\text{wall}} = \text{constant} \tag{12}$$

$$\text{wall (B} - \text{C), (D} - \text{E), (I} - \text{K) and (L} - \text{A)}: \quad \frac{\partial T}{\partial y} = 0. \tag{13}$$

(iii) outlet boundary (E–G), (I–F)

The flow field can be regarded as fully developed when the outlet is located far away from the recirculation region. Thus, all the quantity gradients were zero except the velocity component V, which was zero:

$$\frac{\partial U}{\partial x} = \frac{\partial K}{\partial x} = \frac{\partial \varepsilon}{\partial x} = \frac{\partial T}{\partial x} = 0, \qquad V = 0. \tag{14}$$

(iv) symmetric boundary (A–F)

The symmetric boundary was applied to the case without surface motion,

$$U = 0, \qquad \frac{\partial V}{\partial X} = 0, \qquad \frac{\partial T}{\partial X} = 0. \tag{15}$$

3 Numerical procedure

The numerical method used in the present study is based on the SIMPLE algorithm of Patankar [13]. The conservation equations are discretized by a control volume based finite difference method with power-law scheme. The set of difference equations is solved iteratively

using a line by line solution method in conjunction with a tridiagonal matrix form. Based on the grid independent study, the grid (33 × 97) is used. The solution is considered to be converged when the normalized residual of the algebraic equation is less than a prescribed value of 0.000 1.

4 Discussion

A nonuniform grid arrangement was used in the present computations. The grid system was suggested with the velocity nodes displaced from scalar nodes. Grid independence test was performed with three different grid sizes, namely 22 × 69, 33 × 97, and 40 × 116. The parameter used to check the grid independence of the computational results was the skin friction coefficient as shown in Fig. 4. The calculation solutions appear to be independent for a grid distribution of 33 × 97.

All computations reported here were performed with a mesh consisting of 33 × 97 nonuniformly distributed grid lines based on grid independent test. The velocity vector plots of Fig. 5 provide an overall view of the flow without surface motion. The flow field indicates the presence of two low-pressure recirculation zones being induced by the interaction between the nozzle mainstream and fountain upwash flow. To investigate the effects of Reynolds number on C_f, it was varied from 11 000 to 44 000 while keeping the other

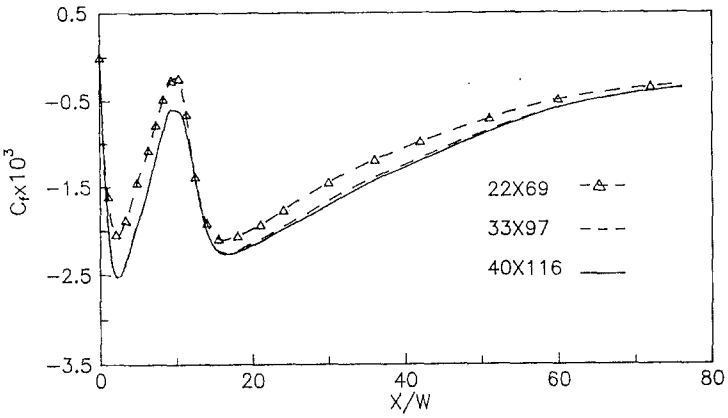

Fig. 4. Effect of grid refinement on skin friction coefficient

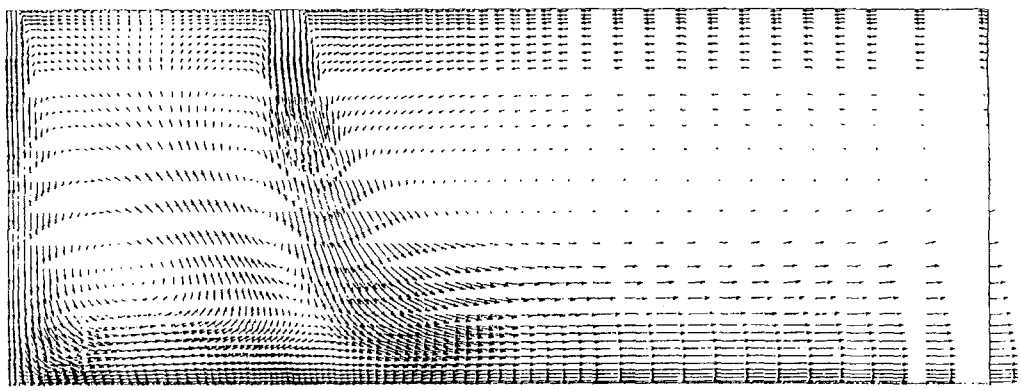

Fig. 5. Velocity vectors

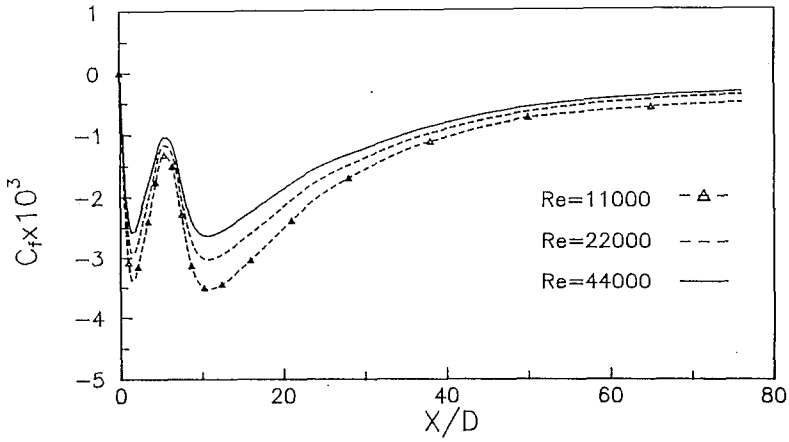

Fig. 6. Reynolds number effects on skin friction coefficient ($H/W = 8$ and $P/W = 5$)

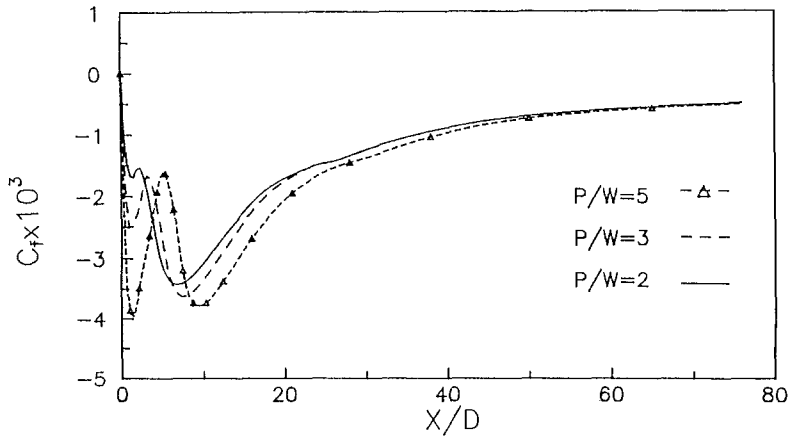

Fig. 7. Pitch effects on skin friction coefficient (Re = 22 000 and $H/W = 6$)

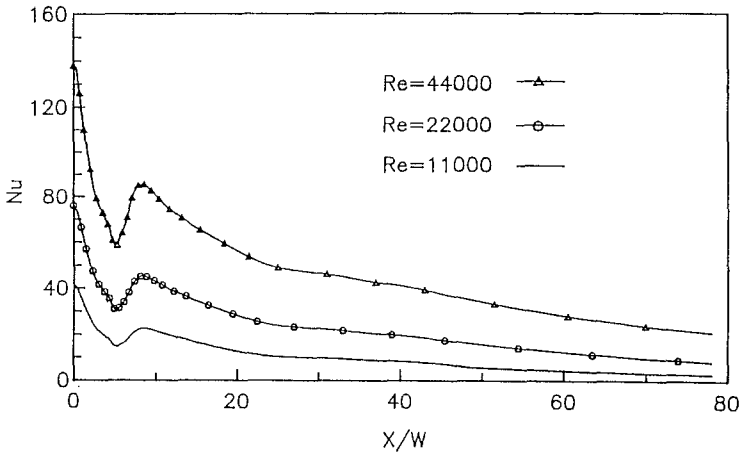

Fig. 8. Reynolds number effects on Nu ($H/W = 8$ and $P/W = 5$)

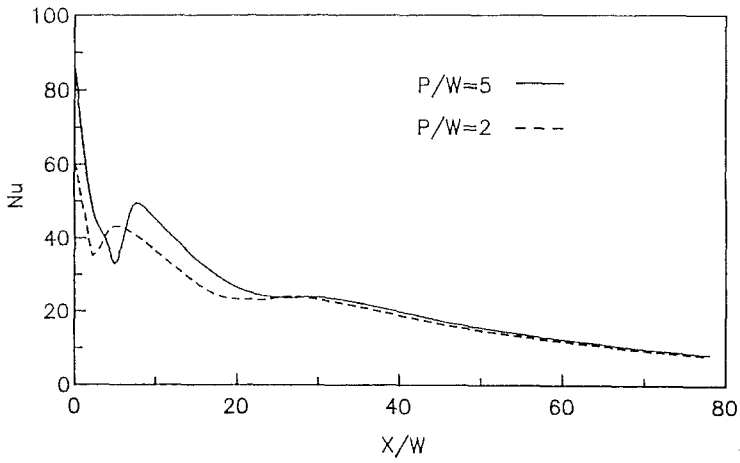

Fig. 9. Pitch effects on Nu (Re = 22000 and $H/W = 6$)

parameters constant, i.e., $H/W = 8$ and $P/W = 5$. The shear stress on the impingement surface is expressed dimensionless as the skin friction coefficient, $C_f = \tau_w/0.5\,\varrho V_j^2$. The predicted C_f was found to have a peak value between the nozzles as shown in Fig. 6. Similarly, to investigate the effects of the pitch, the Reynolds number was fixed at 22000 and $H/W = 6$. The predictions indicate that the location of the first peak value was independent of P/W as shown in Fig. 7.

In Fig. 8, the local Nusselt number distribution is plotted for various values of Re, $H/W = 8$ and $P/W = 5$. The predicted local Nusselt number distribution shows a peak in the stagnation region and a local minimum between the nozzles. Figure 9 shows the effect of nozzle pitch to the local Nusselt number at Re = 22000 and $H/W = 6$. As expected, the maximum value of the local Nusselt number Nu is seen to shift downstream with increasing the nozzle pitch. Downstream of the second jet, the local Nusselt number distribution is nearly the same as that with two different nozzle pitches. The augmentation of heat transfer was divided into two parts, namely, the increase resulting from the increasing flow rate and the impingement of fluid. The effects of surface motion on C_f along the moving surface for three different Reynolds numbers are shown in Fig. 10 a, Fig. 10 b, and Fig. 10 c, respectively. These results show the same conclusion that the shear stress increases with increasing surface motion. Increasing the surface velocity steepens the velocity gradient of the flow near the wall resulting in an increasing shear stress. For the region downstream of the recirculation zone, the direction of the flow is the same as the direction of the surface velocity. In this region, the absolute shear stress decreases. This is due to the fact that the relative motion between the impingement surface and the flow is reduced. However, if the sign convection for shear stress is used, the shear stress also increases. Figure 11 shows the effect of Re for $U_s/V_j = 0.05$, $P/W = 5$, and $H/W = 6$. The increase of Re affects the level of wall shear stress. The position of maximum value of C_f by the second nozzle does not change with Re. Figure 12 shows the effect of surface motion on the local Nusselt number dustribution for Re = 44000, $P/W = 5$, and $H/W = 6$. The predictions show that the heat transfer characteristics are not significant in the cases of $U_s/V_j = 0.25$ and 0.0. The effect of the Reynolds number on the local Nusselt number distribution for $U_s/V_j = 0.05$, $P/W = 5$, and $H/W = 6$ is shown in Fig. 13. As expected, an increase of the jet Reynolds number (Re) enhances the heat transfer coefficient over the entire impingement surface.

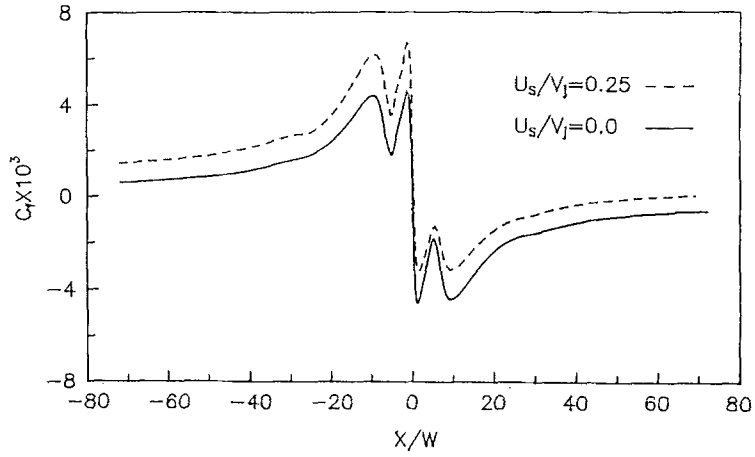

a

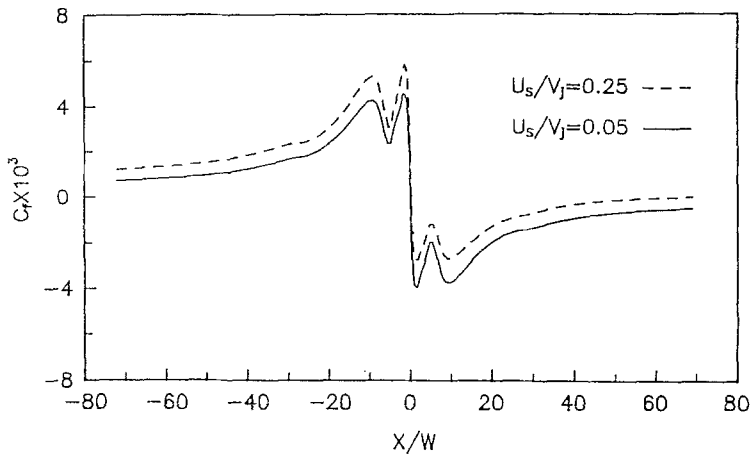

b

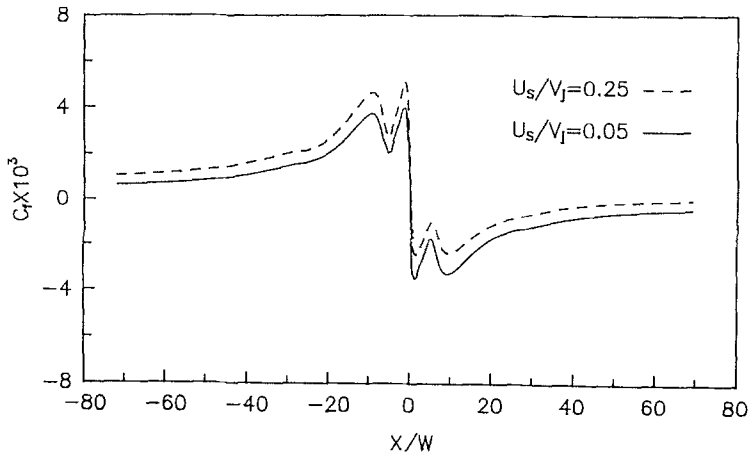

c

Fig. 10. Surface motion effects on skin friction coefficient **a** Re = 11 000, $P/W = 5$ and $H/W = 6$, **b** Re = 22 000, $P/W = 5$ and $H/W = 6$, **c** Re = 44 000, $P/W = 5$ and $H/W = 6$

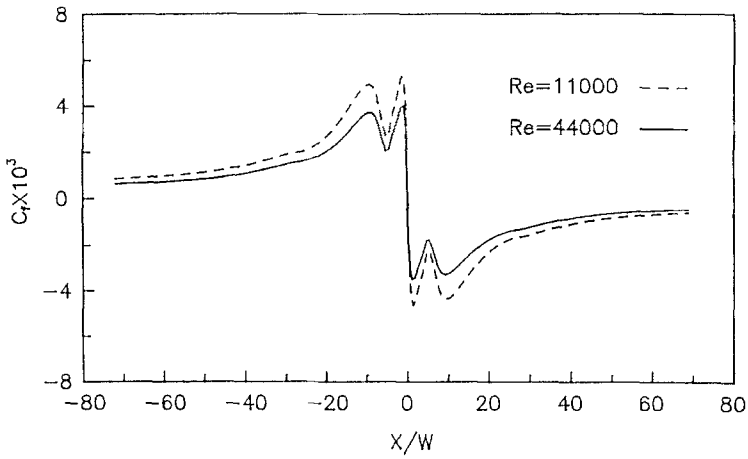

Fig. 11. Reynolds number effects on skin friction coefficient ($U_s/V_j = 0.05$, $H/W = 6$ and $P/W = 5$)

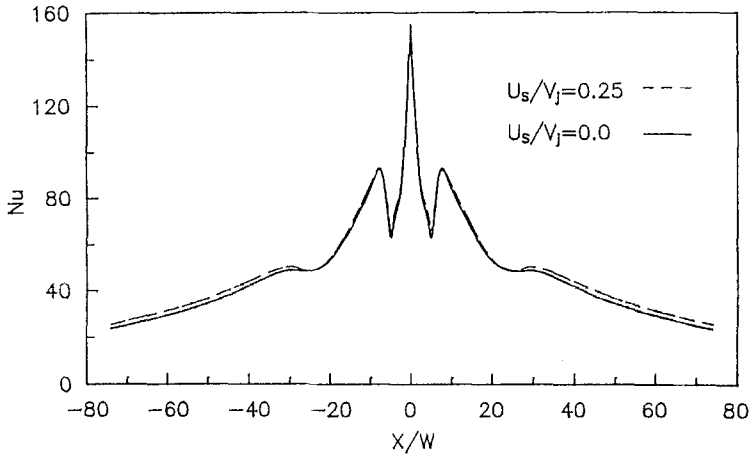

Fig. 12. Surface motion effects on Nu (Re = 44 000, $P/W = 5$ and $H/W = 6$)

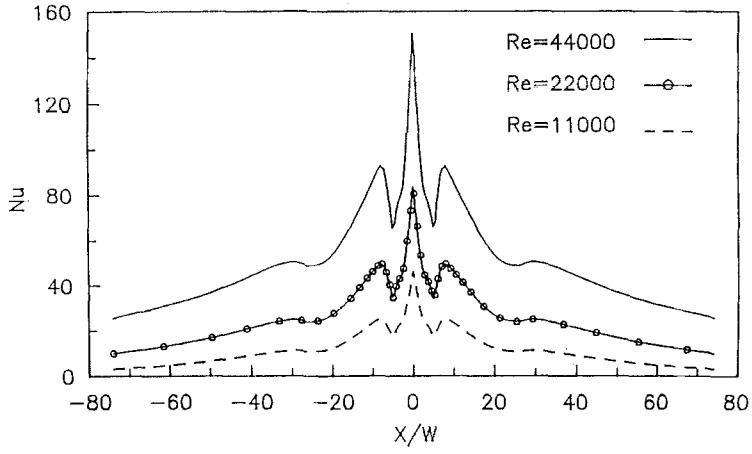

Fig. 13. Reynolds number effects on Nu ($U_s/V_j = 0.05$, $H/W = 6$ and $P/W = 5$)

5 Conclusion

The fluid flow and heat transfer characteristics for three turbulent slot jets are presented. The interference effects are enhanced when the jets are closely spaced, the separation distance between the jet orifices is small, and when the impingement surface is relatively large. The other interaction is the collision of the surface flows (i.e., the wall jets) associated with adjacent impinged jets. These collisions are expected to be of increasing importance when the jets are closely spaced, the jet orifice-impingement surface separation is small, and the jet velocity is large.

In the design of multiple jet impingement systems, the geometrical and the flow parameters have to be selected to attain both a sufficiently high average heat transfer coefficient and a degree of uniformity in the surface distribution that is adequate to avoid local hot (or cold) spots. This paper provides a basic study to design multiple impingement jets.

Acknowledgment

We would like to thank the National Science Council of the Republic of China for support of this work under contract NO. NSC 83-0401-E-006-123.

References

[1] Wolfstein, M.: Some solutions of the plane turbulent impinging jet. ASME J. Basic Engng. **92,** 915–922 (1970).
[2] Bower, W. W., Kotansky, D. R., Hoffman, G. H.: Computations and measurements of two-dimensional turbulent jet impingement flowfields. Symposium on Turbulent Shear Flows, NO. 3.1, Penn. State University, Pennsylvania 1977.
[3] Gosman, A. D., Pun, W. M., Runchal, A. K., Spalding, D. B., Wolfstein, M.: Heat and mass transfer in recirculating flows, pp. 192–198. Academic Press 1969.
[4] Spalding, D. B.: Heat transfer from turbulent separated flows. J. Fluid Mech. **27,** 97–109 (1967).
[5] Agarwal, R. K., Bower, W. W.: Navier-Stokes computations of turbulent compressible two-dimensional impinging jet field. AIAA J. **20,** 577–584 (1982).
[6] Huang, P. G., Majumdar, A. S., Douglas, W. J. M.: Numerical prediction of fluid flow and heat transfer under a turbulent impinging slot jet with surface motion and crossflow. ASME paper 84-WA/HT-33, 1984.
[7] Amano, R. S., Brandt, H.: Numerical study of turbulent axisymmetric jets impinging on a flat plate and flowing into an axisymmetric cavity. Trans. ASME, J. Fluids Engng. **106,** 410–418 (1984).
[8] Chuang, S. H., Wei, C. Y.: Computations for a jet impinging obliquely on a flat surface. Int. J. Num. Meth. Fluids **12,** 637–653 (1991).
[9] Chuang, S. H., Chen, M. H., Li, S. W., Tai, F. M.: Numerical simulation of twin-jet impingement on flat plate coupled with cross-flow. Int. J. Num. Meth. Fluids **14,** 459–475 (1992).
[10] Reizes, J. A. (ed.): Transport phenomena in heat and mass transfer **1,** 456–467 (1992).
[11] Launder, B. E., Spalding, D. B.: The numerical computation of turbulent flows. Comp. Meth. Appl. Mech. Engng. **3,** 269–289 (1974).
[12] Jayatilleke, C. L.: The influence of Prandtl number and surface roughness on the resistance of the laminar sublayer to momentum and heat transfer. Prog. Heat Mass Transfer **1,** 193–329 (1969).
[13] Patankar, S. V.: Numerical heat transfer and fluid flow. New York: Mc Graw-Hill 1980.

Authors' address: Prof. Y.-T. Yang and T.-P. Hao, Department of Mechanical Engineering, National Cheng Kung University, Tainan, Taiwan, 701, R.O.C.